Electrochemical Preparation of Poly(5-cyanoindole)/carbon Fiber Core/Shell Structure Composite and Its Capacitance Performance

Xiumei Ma[1,§], Weiqiang Zhou[1,§], Daize Mo[1], Jian Hou[2], Jingkun Xu[1,]*

[1] Jiangxi Key Laboratory of Organic Chemistry, Jiangxi Science and Technology Normal University, Nanchang 330013
[2] State key laboratory for marine corrosion and protection，Luoyang ship material research institute, Qingdao, 266101, China
[*]E-mail: xujingkun@tsinghua.org.cn
§ Xiumei Ma and Weiqiang Zhou, These authors contributed equally to this work.

Poly(5-cyanoindole)/carbon fiber composite material (P5CIn/CF) was prepared via a simple electrodeposition method. The CF core and the P5CIn shell formed a 3-D P5CIn/CF core/shell structure composite. The P5CIn/CF was characterized by FT-IR spectroscopy, scanning electron microscope, cyclic voltammetry, electrochemical impedance spectroscope, and galvanostatic charge/discharge techniques. The specific capacitance of P5CIn/CF was 302 F g^{-1} at the scan rate of 1 A g^{-1}. The assembled symmetric supercapacitor based on P5CIn/CF showed a specific capacitance of 94 F g^{-1} at 7.5 mV s^{-1} and its energy density reached 16 Wh kg^{-1} at the power density of 0.6 kW kg^{-1}. Additionally, the capacitance retention of P5CIn/CF was 78% after 2000 cycles. These results suggested that the P5CIn/CF was a hopeful electrode material for the flexible supercapacitors application.

1. INTRODUCTION

The dramatic development of portable electronic devices and hybrid electric vehicles has created a large demand for innovative energy storage materials of high power density and efficient energy conversion [1-6]. Supercapacitors are outstanding energy storage devices with excellent capacitance performance. Compared with rechargeable batteries, they have significantly higher power

densities and much better cyclic stability, therefore, they are widely considered as one of the most hopeful technologies for next-generation energy storage. Based on the involved energy storage mechanism, there are two kinds of supercapacitors: (1) electrical double layer capacitors (EDLC) based on ion adsorption, (2) pseudocapacitors based on electrochemical redox reactions [7].

As an important type of supercapacitor, EDLC generally uses carbon materials with high surface area as electrode material. In general, carbon materials such as activated carbon [8], carbide-derived carbons [9,10], ordered mesoporous carbons [11,12], carbon aerogels [13], carbon nanotubes [14-16], and grapheme [17] are widely used for EDLC. Nevertheless, most of them exist in powder forms hence assembling them into electrodes usually needs using binders, conducting additives and current collectors [18,19]. Employing these additional components has brought in a large processing cost and amount of compromises in the electrode-level performance metrics have now been recognized. In addition, the procedures to fabricate supercapacitor with carbon nanotubes, carbon onions and grapheme need high cost and are difficult for mass production and/or require complicated processes to assemble electrodes. Carbon fiber cloth (CF), which is a cost effective and highly conductive textile with outstanding mechanical flexibility and strength, and intrinsic electrically conductive networks for electronic transport and porous structures for efficient ionic diffusion, was used as both substrate and current collector to achieve flexibility [20].

Pseudocapacitive polymers including polypyrrole (PPy), polyaniline (PANI), polythiophene (PTh) and their derivatives have attracted extensive investigation as active electrode materials for supercapacitors due to their high energy density and large charge transfer-reaction pseudocapacitance based on fast and reversible redox reactions at the electrode surface, leading to significantly enhanced specific capacitance which exceeds that of carbon-based materials [21]. Due to the complementary mechanical, electrical and electrochemical properties, CPs has been investigated intensely in combination with CF. For example, Cheng et al. reported PANI nanowires which were coated on electro-etched carbon fiber [22]. The PANI nanowires had a specific capacitance of 673 F g^{-1}. Kim et al. reported that PPy nanofilms were deposited on carbon fibers via an in situ chemical polymerization technique [23]. This PPy nano-layer displayed higher specific capacitance up to 545 F g^{-1} ~ 588 F g^{-1} along with an excellent power capability. Chu et al. reported that PEDOT was potentiostatically grown on carbon fiber with an optimal deposition time of 20 mins, leading to a high specific capacitance value, i.e., 126.23 F g^{-1} [24]. However, there are no report about the composite of carbon fiber cloth with polyindoles used for supercapacitor electrode. Among polyindoles, the cyano-subsitituted polyindole are good active electrode materials for supercapacitors [25]. In addition, the grafting of cyano group with high electron affinity gives rise to a considerable positive shift in reduction potential and afford low band gap polymers [26,27].

In this paper, we prepared a poly(5-cyanoindole)/carbon fiber (P5CIn/CF) core/shell structure composite through a one-step electrodeposition without involving any additional binders, conductive additives or complicated electrode processing steps. As-prepared P5CIn shell was homogeneously coated on the CF. The porous network CF will increase the specific surface area of P5CIn, and thus improve the capacitance performance of P5CIn. The electrochemical performance of composite was examined by cyclic voltammograms, galvanostatic charge/dischargeand electrochemical impedance spectroscopy methods in 1.0 M H_2SO_4 solution.

2. EXPERIMENTAL

2.1. Materials

Carbon fiber cloth (W0S1002, Ce Tech) with a thickness of about 360 µm was consisting of carbon fibers with a diameter of 10 µm, which was purchased from Phychemi Company Limited, China. Acetonitrile (ACN, Beijing Chemical Plant, China), 5-cyanoindole (5CIn, Shandong Pingyuan Hengyuan Chemical Co., Ltd., China), lithium perchlorate (LiClO$_4$, AR, Xiya Reagent Research Center), sulfuric acid (H$_2$SO$_4$, 98%, Xilong Chemical) were used as received without further purification.

2.2. Apparatus

The electrochemical experiments were performed by a CHI 660B potentiostat/galvanostat, which was purchased from Shanghai Chenhua Instrumental Co., Ltd., China. Impedance spectra were carried out at an ac amplitude of 5 mV and the data were obtained in the frequency range 10^5 to 10^{-2} Hz. The reference electrode and the counter electrode were saturated calomel electrode (SCE) and platinum wire (1 mm diameter), respectively. Scanning electron microscope (SEM) tests were carried out using scanning electron microscope (JSM-5600, JEOL). Infrared spectra were recorded with a Bruker Vertex 70 Fourier transform infrared (FT-IR) spectrometer with samples in KBr pellets.

2.3 Preparation of P5CIn/CF electrode

The polymer films were prepared potentiostatically on CF substrates at 1.43 V in ACN solution which contains 50 mM 5CIn and 0.1 M LiClO$_4$. The polymer film mass (W_p) was calculated according to eq. (1): [28]

$$W_p = \frac{(\eta Q_{dep})(M)}{FZ} \qquad (1)$$

Herein, W_p is calculated by using the charge (Q_{dep}), assuming a 100% current efficiency (η) (the total charge passed through the cell during the polymer film preparation process). F is the Faraday constant (96485 C/mol), M is the molecular weight of 5CIn. Z is the number of electrons transferred per monomer affiliated to the polymer, in which $Z = 2 + f$ [29,30]. The partial charge f is called the doping level, which was about 0.23 in here, assuming a 100% current efficiency, according to eq. (2): [31]

$$f = \frac{2Q_o}{Q_d - Q_o} \qquad (2)$$

Where Q_d is the total charge employed in depositing process, and Q_o is the total charge of oxidized species in the P5CIn films.

2.4 Preparation of symmetric supercapacitor

The supercapacitor was simply constructed with two symmetrical P5CIn/CF electrodes as negative electrode and positive electrode, respectively. The electrolyte used for the above supercapacitor was 1.0 M H_2SO_4 aqueous solution.

2.5 Capacitance calculation

Specific capacitance (*C*) of P5CIn electrode and supercapacitor were calculated from cyclic voltammograms (CVs) by eq. (3): [32]

$$C = \frac{\int_{E_1}^{E_2} i(E)\,d(E)}{2vm(E_2 - E_1)} \qquad (3)$$

Where E_1 and E_2 are the cutoff potentials in CV, $i(E)$ is the instantaneous current, $\int_{E_1}^{E_2} i(E)\,d(E)$ is the total voltammetric charge calculated by integration of the positive and negative sweeps in the CVs, *m* is the mass of the individual sample, and *v* is the scan rate.

For the charge-discharge method, the specific capacitance can be obtained according to the eq. (4): [33]

$$C = \frac{It}{mV} \qquad (4)$$

In here, *C* is specific capacitance (F g^{-1}), *I* is discharge current, and *t* is the discharge time. *m* is the mass loading of P5CIn on CF substrates, and *V* is the potential range. For symmetric supercapacitor, the specific capacitance was obtained using the total mass loading of P5CIn on the two electrodes.

For the symmetric supercapacitor, the power density (*P*, W kg^{-1}) and energy density (*E*, Wh kg^{-1}) values can be calculated by the eq. (5 & 6) [34].

$$E = \frac{1}{2}CV^2 \qquad (5)$$

$$P = \frac{E}{\Delta t} \qquad (6)$$

Here, *C* is the specific capacitance of the symmetric supercapacitor, *V* and Δt are the voltage range and discharge time, respectively.

3. RESULTS AND DISCUSSION

3.1 Structural characterizations

Vibrational spectrum can give structural information of conducting polymers. As can be seen from Figure 1, the band at 1451 cm^{-1} and 1625 cm^{-1} were due to the stretching vibration of C-C and C=C, respectively. The band at around 2221 cm^{-1} was the stretching vibration of the CN group. The

band at 1183 cm^{-1} was the vibrational modes of the dopant ClO_4^- in polymer. The band at 841 cm^{-1} in the spectrum was attributed to the three adjacent C-H deformation vibration of ring hydrogens on benzenic ring, indicating that the benzene ring on P5CIn unit was 1,2,4-tri-substitution, which proved that the polymerization of 5CIn took place at the pyrrole ring. Additionally, the narrow peak at 3685 cm^{-1} was the characteristic absorption of the N-H bond, together with the one at 1551 cm^{-1}, were result from the elongation and the deformation vibrations of the N-H bond, respectively, which implied the existence of N-H bonds on the P5CIn main chain. Therefore, nitrogen species could not be the polymerization sites and the P5CIn film polymerized at the C_2 and C_3 positions.
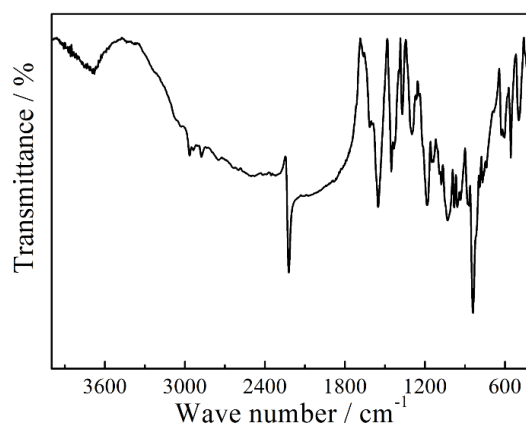
Figure 1. FT-IR spectrum of P5CIn.

3.2. Morphology
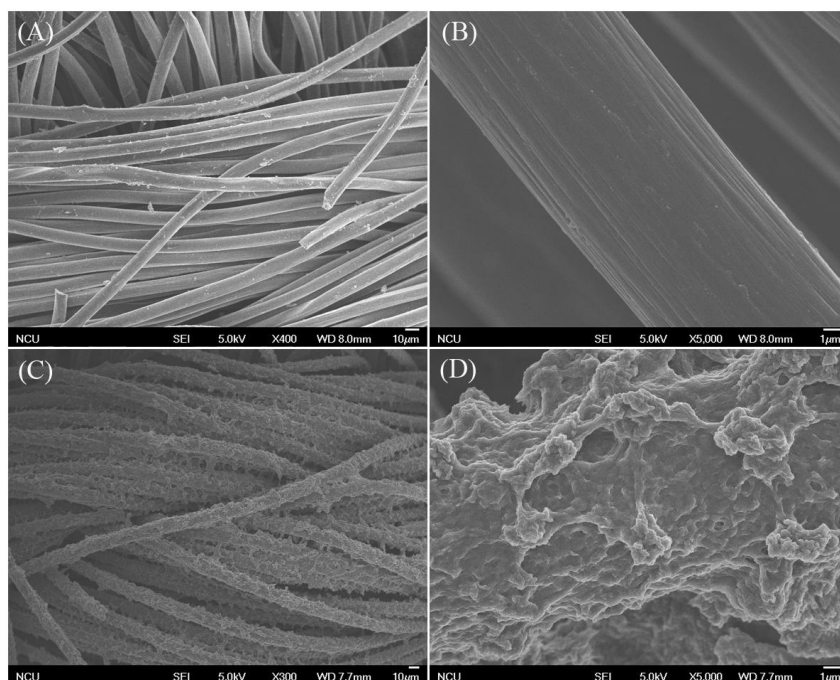
Figure 2. SEM of bare CF (A, B) and P5CIn/CF (C, D).

Figure 2 shows the SEM images of CF (A&B) and P5CIn/CF (C&D). As displayed in Figure 2A, the carbon fiber cloth is consisting of many CF that arranged crosswise to form a 3-D structure with numerous spaces, forming a 3-D highly porous structure, which was benefit for the fast transport of electrons and ions in the supercapacitor devices. And the CF had smooth surface (Figure 2B). SEM image of P5CIn/CF indicated that a rough P5CIn film was homogeneously coated on the surface of CF, forming a 3-D core/shell structure (Figure 2C). This morphological structure has the following advantages acting as the supercapacitors electrode: (1) the 3-D highly space structure promotes de-polarisation of the ion concentration and hence leading to a high speed of charge–discharge, and the space leads to a high interfacial area and therefore a high specific capacitance. (2) The 3-D core/shell structure creates efficient diffusion paths for electrolyte ions that would remarkably accelerate intercalation of ions and enhance the efficiency of the usage rate of electrode materials.

3.3. Electrochemical properties of P5CIn/CF
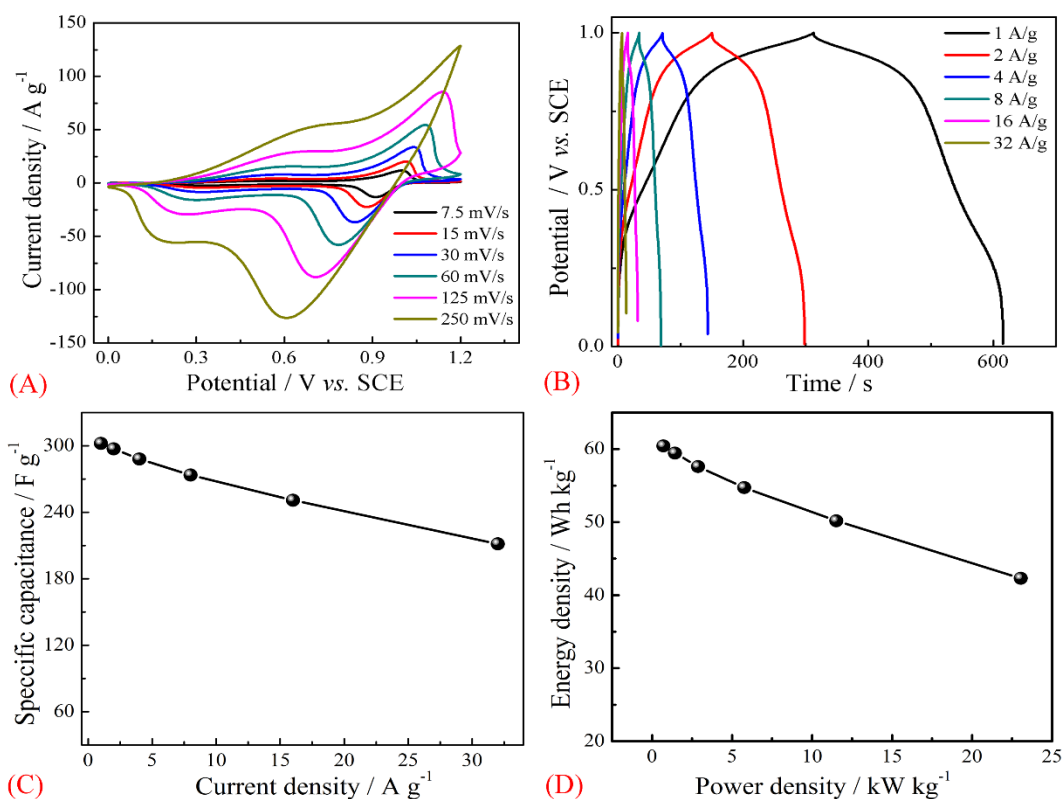
Figure 3. (A) CVs of P5CIn/CF electrode in 1.0 M H_2SO_4 solution at different potential scan rates, (B) Galvanostatic charge/discharge curves of P5CIn/CF electrode in 1.0 M H_2SO_4 solution at different current density, (C) Specific capacitance as a function of current density, (D) Power density as a function of energy density.

The CV curves of the electrode at different scan rates from 7.5 to 250 mV s^{-1} were shown in Figure 3A. The CV curves of P5CIn/CF electrode in 1.0 M H_2SO_4 presented two couple of anodic and

cathodic peaks, showing big differences from that of electric double layer capacitance in which case it was normally close to an ideal rectangular shape, suggesting that the charge capability of P5CIn/CF electrode is due to its ability to undergo electro-oxidation and electro-reduction [35,36]. The shape of the curves had no evident changes even at a relative higher scan rate of 250 mV s^{-1}, revealing the good kinetic reversibility of the electrodes. Moreover, the cathodic peak potentials (E_{pc} values) shifted negatively and the anodic peak potential (E_{pa} value) shifted positively with increasing scan rate, which resulted mainly from the resistance of the electrode. Furthermore, the obvious peak current density increase with the scan rates indicated the good rate ability for the P5CIn/CF electrode.

Figure 3B displays the charge-discharge curves of P5CIn/CF electrode at different current densities. The shape of charge-discharge curves were similar between 0 and 1.0 V, suggesting that the P5CIn/CF electrode can be stably operated in this range of current densities. Figure 3C displays the specific capacitance of P5CIn/CF electrode obtained by equation (4) at different current densities. The specific capacitance was 302 F g^{-1} at a current density of 1 A g^{-1}, and still retained at 212 F g^{-1} when a relative higher current density of 32 A g^{-1} was employed. For further investigation of the capacitive performance of P5CIn/CF electrode, the power density and energy density values were obtained by eq. (5&6) (Figure 3D). The energy density of 60 Wh kg^{-1} was obtained at a power density of 0.7 kW kg^{-1}, and when the power density increased to 23 kW kg^{-1}, the energy density still reached 42 Wh kg^{-1}.
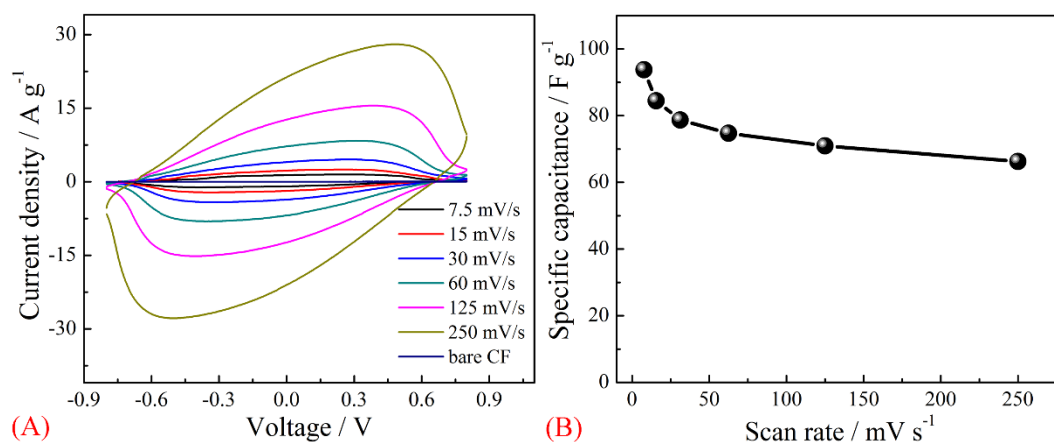
Figure 4. (A) CVs of symmetric supercapacitor based on P5CIn/CF electrodes at different potential scan rates and the bare CF electrode at a scan rate of 250 mV s^{-1}; (B) Specific capacitance as a function of scan rates.

To evaluate further the advantage of the P5CIn/CF as electrode material, symmetric supercapacitor based on P5CIn/CF electrode was assembled. The CV curves of the supercapacitor at scan rates range from 7.5 to 250 mV s^{-1} were showed in Figure 4A. The shape of the curves have no obvious difference even at the relative higher scan rate of 250 mV s^{-1}, suggesting the good kinetic reversibility of the supercapacitor. The significant increase of peak current density with the increase of scan rates indicated the good rate ability for the symmetric supercapacitor. In comparison with P5CIn/CF electrode, the specific capacitance of bare CF was negligible. Figure 4B shows the specific capacitance of P5CIn/CF electrode at different potential scan rates. The specific capacitance reached

94 F g^{-1} at a scan rate of 7.5 mV s^{-1}, and remained at 66 F g^{-1} when the scan rate reached up to 250 mV s^{-1} was used.
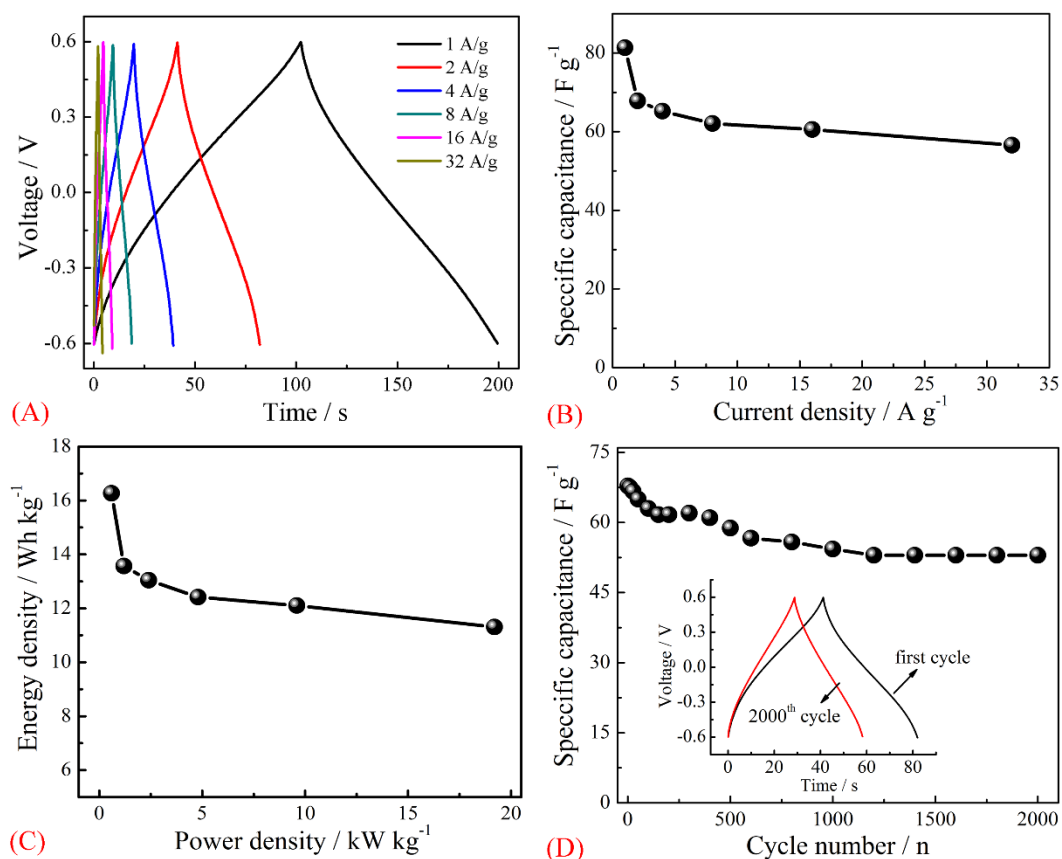
Figure 5. (A) Galvanostatic charge/discharge curves of the symmetric supercapacitor based on two P5CIn/CF electrodes in 1.0 M H$_2$SO$_4$ solution at different current density. Voltage range between -0.6 V and 0.6 V; (B) Specific capacitance as a function of current density; (C) Ragone plot; (D) Cycling performance during 2000 cycles at a current density of 2.0 A g^{-1}.

The charge/discharge measurements were performed at various current densities from -0.6 V to 0.6 V. As displayed in Figure 5A, when the current density ranged from 1 to 32 A g^{-1}, the shape of charge-discharge curves have no obvious change. As seen from Figure 5B, the specific capacitance of the symmetric supercapacitor was 81 F g^{-1} at 1 A g^{-1}, with the increasing of current density, the specific capacitance decreased to 57 F g^{-1} at 32 A g^{-1}. Figure 5C showed the energy density of the symmetric supercapacitor as a function of power density. The energy density was 16 Wh kg^{-1} at a power density of 0.6 kW kg^{-1} and decreased to 11 Wh kg^{-1} when the power density reached 19.2 kW kg^{-1}.

The cycling ability, another vital parameter for electrode materials as supercapacitors [37], was shown from the specific capacitance as a function of cycle number based on charge-discharge curves at the current density of 2 A g^{-1}. As shown in Figure 5D, the shape of the charge-discharge curve at the first and 2000th cycle (inset of Figure 5D) were similar, and the specific capacitance of the symmetric supercapacitor was 68 F g^{-1} at the first cycle, and then slowly decreased to 54 F g^{-1} at the 1000th

cycle, subsequently, achieved a steady capacitance value of 53 F g^{-1}, with a total loss of 22% after 2000 cycles. This result suggested the good cycle ability of the symmetric supercapacitor based on P5CIn/CF electrodes.
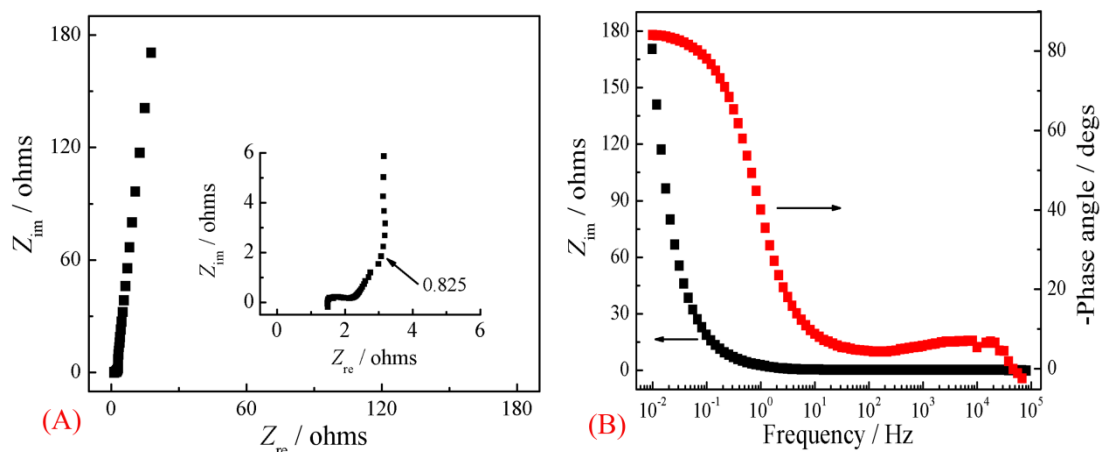
Figure 6. Impedance spectra of the symmetric supercapacitor based on two P5CIn/CF electrodes in 1.0 M H$_2$SO$_4$ solution: (A) Nyquist plots; (B) Bode-phase angle plots. Electrode potential: 0 V.

In order to further test the electrochemical performance of the symmetric supercapacitor based on two P5CIn/CF electrodes, an electrochemical impedance spectroscopy test was implemented at 0 V. Figure 6 displays the impedance spectra of the symmetric supercapacitor in 1.0 M H$_2$SO$_4$ solution. As shown in Figure 6A, the impedance curves display a nearly vertical straight line in the low frequency region and a flattened semicircle in the high frequency region. The knee frequency (*f*) at the phase angle of -45° is an vital parameter to evaluate the speed of charge-discharge process of films [38], and it was 0.825 Hz of the supercapacitor based on P5CIn/CF electrode, indicating that a pure capacitive behavior was received and most of its stored energy was accessible at frequencies below this value [30]. The impedance of the electrolyte, evaluated by the intercepts of the Nyquist curves on the real axis, was about 1.5 ohm. Moreover, the diameter of the impedance arc was about 0.85 ohm, suggesting the small charge-transfer resistance of the symmetric supercapacitor. In the phase angle plot (Figure 6B), the phase angle approaching to -90º at low frequency is an evidence of the pure capacitive behavior. The phase angle of P5CIn/CF electrode was -84º at 0.01 Hz, which indicated the good capacitive performance of the symmetric supercapacitor based on two P5CIn/CF electrodes.

4. CONCLUSION

In this paper, P5CIn was electrodeposited onto the surface of CF without involving any binders, conductive additives or complicated electrode processing steps. According to FTIR-IR, P5CIn was prepared mainly via the coupling of 5CIn at C$_2$ and C$_3$ positions. SEM proved that as-prepared P5CIn was homogeneously coated on the surface of CF. The electrochemical results displayed that the

specific capacitance of P5CIn/CF reached up to 302 F g^{-1} at 1 A g^{-1} in 1.0 M H$_2$SO$_4$ solution. The specific capacitance of symmetric supercapacitor based on P5CIn/CF reached 81 F g^{-1} at 1 A g^{-1} and the energy density was 16 Wh kg^{-1} at a power density of 0.6 kW kg^{-1}. Additionally, the capacitance retention of P5CIn/CF was 78% after 2000 cycles. These results showed that the P5CIn/CF core/shell structure composite material can be used as a potential electrode material for supercapacitor.

Reference

1. W.L. Song, K. Song, L.Z. Fan, *Acs Appl. Mater. Inter.*, 7 (2015) 4257-4264.
2. J.R. Miller, P. Simon, *Science Magazine*, 321 (2008) 651-652.
3. P. Simon, Y. Gogotsi, *Nat. Mater.*, 7 (2008) 845-854.
4. G. Wang, L. Zhang, J. Zhang, *Chem. Soc. Rev.*, 41 (2012) 797-828.
5. P. Simon, Y. Gogotsi, *Accounts Chem. Res.*, 46 (2012) 1094-1103.
6. Y. Zhai, Y. Dou, D. Zhao, P.F. Fulvio, R.T. Mayes, S. Dai, *Adv. Mater.*, 23 (2011) 4828-4850.
7. H. Wang, Y. Liang, T. Mirfakhrai, Z. Chen, H.S. Casalongue, H. Dai, *Nano Res.*, 4 (2011) 729-736.
8. A. Burke, *Electrochim. Acta*, 53 (2007) 1083-1091.
9. J. Chmiola, G. Yushin, Y. Gogotsi, C. Portet, P. Simon, P.L. Taberna, *Science*, 313 (2006) 1760-1763.
10. C. Portet, M.Á. Lillo-Ródenas, A. Linares-Solano, Y. Gogotsi, *Phys. Chem. Chem. Phys.*, 11 (2009) 4943-4945.
11. W. Xing, S. Qiao, R. Ding, F. Li, G. Lu, Z. Yan, H. Cheng, *Carbon*, 44 (2006) 216-224.
12. K. Jurewicz, C. Vix-Guterl, E. Frackowiak, S. Saadallah, M. Reda, J. Parmentier, J. Patarin, F. Béguin, *J. Phys. Chem. Solids*, 65 (2004) 287-293.
13. R. Pekala, J. Farmer, C. Alviso, T. Tran, S. Mayer, J. Miller, B. Dunn, *J. Non-Cryst. Solids*, 225 (1998) 74-80.
14. D.N. Futaba, K. Hata, T. Yamada, T. Hiraoka, Y. Hayamizu, Y. Kakudate, O. Tanaike, H. Hatori, M. Yumura, S. Iijima, *Nat. Mater.*, 5 (2006) 987-994.
15. E. Frackowiak, F. Beguin, *Carbon*, 40 (2002) 1775-1787.
16. C. Niu, E.K. Sichel, R. Hoch, D. Moy, H. Tennent, *Appl. Phys. Lett.*, 70 (1997) 1480-1482.
17. T. Kim, G. Jung, S. Yoo, K.S. Suh, R.S. Ruoff, *ACS Nano*, 7 (2013) 6899-6905.
18. Z. Fan, J. Yan, L. Zhi, Q. Zhang, T. Wei, J. Feng, M. Zhang, W. Qian, F. Wei, *Adv. Mater.*, 22 (2010) 3723-3728.
19. J. Gamby, P. Taberna, P. Simon, J. Fauvarque, M. Chesneau, *J. Power Sources*, 101 (2001) 109-116.
20. L. Wang, X. Feng, L. Ren, Q. Piao, J. Zhong, Y. Wang, H. Li, Y. Chen, B. Wang, *J. Am. Chem. Soc.*, 137 (2015) 4920-4923.
21. G. Yu, L. Hu, N. Liu, H. Wang, M. Vosgueritchian, Y. Yang, Y. Cui, Z. Bao, *Nano Lett.*, 11 (2011) 4438-4442.
22. Q. Cheng, J. Tang, J. Ma, H. Zhang, N. Shinya, L.C. Qin, *J. Phys. Chem. C*, 115 (2011) 23584-23590.
23. J.H. Kim, A.K. Sharma, Y.S. Lee, *Mater. Lett.*, 60 (2006) 1697-1701.

24. C.Y. Chu, J.T. Tsai, C.L. Sun, *Int. J. Hydrogen Energ.*, 37 (2012) 13880-13886.
25. W. Zhou, X. Ma, F. Jiang, D. Zhu, J. Xu, B. Lu, C. Liu, *Electrochim. Acta*, 138 (2014) 270-277.
26. L. Gao, W. Senevirathna, G. Sauve, *Org. Lett.*, 13 (2011) 5354-5357.
27. J. Xu, W. Zhou, H. Hou, S. Pu, L. Yan, J. Wang, *Mater. Chem. Phys.*, 99 (2006) 341-349.
28. W. Zhou, Y. Du, H. Zhang, J. Xu, P. Yang, *Electrochim. Acta*, 55 (2010) 2911-2917.
29. X. Ma, W. Zhou, D. Mo, Z. Wang, J. Xu, *Synthetic Met.*, 203 (2015) 98-106.
30. X. Ma, W. Zhou, D. Mo, K. Zhang, Z. Wang, F. Jiang, D. Hu, L. Dong, J. Xu, *J. Electroanal. Chem.*, 743 (2015) 53-59.
31. X. Ma, W. Zhou, D. Mo, B. Lu, F. Jiang, J. Xu, *RSC Adv.*, 5 (2015) 3215-3223.
32. M.E. Plonska-Brzezinska, M. Lewandowski, M. Blaszyk, A. Molina-Ontoria, T. Lucinski, L. Echegoyen, *Chemphyschem*, 13 (2012) 4134-4141.
33. M.D. Stoller, R.S. Ruoff, *Energ. Environ. Sci.*, 3 (2010) 1294-1301.
34. H.B. Wu, H. Pang, X.W. Lou, *Energ. Environ. Sci.* 6 (2013) 3619-3626.
35. Y.Z. Zheng, H.Y. Ding, M.L. Zhang, *Mater. Res. Bull.*, 44 (2009) 403-407.
36. Y. Xiao, C. Long, M.T. Zheng, H.W. Dong, B.F. Lei, H.R. Zhang, Y.L. Liu, *Chinese Chem. Lett.*, 25 (2014) 865-868.
37. M.J. Shi, S.Z. Kou, B.S. Shen, J.W. Lang, Z. Yang, X.B. Yan, *Chinese Chem. Lett.*, 25 (2014) 859-864.
38. L. Yuan, X.H. Lu, X. Xiao, T. Zhai, J. Dai, F. Zhang, B. Hu, X. Wang, L. Gong, J. Chen, C. Hu, Y. Tong, J. Zhou, Z.L. Wang, *ACS Nano*, 6 (2012) 656-661.